

# EFFECT OF SURFACE TREATMENT AND ADHEREND MICROSTRUCTURE ON THE FRACTURE TOUGHNESS OF ADHESIVE BONDED NCF COMPOSITES

Alfano, M<sup>1,2</sup>, Montesano, J<sup>2</sup>, Gao, T<sup>2</sup> and Chitsaz Dehaghani, R<sup>2</sup>

<sup>1</sup> DISMI, University of Modena and Reggio Emilia, Reggio Emilia, Italy

<sup>2</sup> Department of Mechanical and Mechatronics Engineering, University of Waterloo, Waterloo, Canada

\* Corresponding author ([marco.alfano@unimore.it](mailto:marco.alfano@unimore.it) | [marco.alfano@uwaterloo.ca](mailto:marco.alfano@uwaterloo.ca))

**Keywords:** *CFRPs; adhesive bonding; toughness*

## ABSTRACT

We investigate the bonding process of carbon-fiber reinforced laminate adherends made via high-pressure resin transfer molding (HP-RTM) with a snap-cure epoxy matrix and non-crimp fabric (NCF) textile. Structural adhesives offer a solution for efficient CFRP joining, but understanding the relationship between surface modification, microstructure, and bond toughness is crucial. We assess surface preparation and bonding processes using double cantilever beam (DCB) and edge notch flexure (ENF) tests. Results of mechanical tests in Mode I and Mode II in conjunction with microscopic fracture surface analysis reveal the significant effect of surface morphology and composition on the mechanisms of failure.

## 1 INTRODUCTION

The increasing demand for high-performance composite materials is expanding beyond traditional applications in aerospace and automotive vehicles [1]. As the demand for composites surges, a concomitant need arises for suitable joining methods. Among these, adhesive bonding has emerged as an appealing technology. Nevertheless, a persistent concern revolves around surface preparation before bonding, particularly considering the expanding array of composites accessible in the market. The evolving architecture and composition of these composites can have a discernible impact on the joining process and emphasizes the critical role of effective surface preparation in ensuring robust and durable adhesive bonds.

In this paper, our primary focus lies in the adhesive bonding process of unidirectional non-crimp fabric (UD-NCF) carbon-fiber reinforced snap-cure epoxy laminate adherends fabricated via high-pressure resin transfer molding (HP-RTM). While HP-RTM holds promise for incorporating CFRPs into high-volume production vehicles, its application in load-bearing structures encounters challenges in efficient CFRP joining. Structural adhesives offer a valuable solution to overcome this hurdle. However, addressing the intricate relationship between surface modification, near-surface adherends' microstructure, and bond toughness is essential for achieving resilient and durable joints. Our study bridges this gap by exploring the mechanical properties of NCF-composites joints bonded with a toughened epoxy adhesive. The effect of surface preparation, bonding processes, and mechanical testing is assessed using the double cantilever beam (DCB) and the edge notch flexure (ENF) test configurations for the CFRP substrates bonded with a toughened epoxy adhesive.

## 2 MATERIALS AND TESTING METHODS

### 2.1 Materials

The NCF composite material used for the joint adherends comprised the UD-NCF PX35-UD300 (Zoltek™) and the three-part snap-cure epoxy TRAC 6150 (Westlake Epoxy). The fabric comprised 5 mm wide carbon fiber tows, each containing 50,000 PX35 carbon fibers, which were stitched with polyester yarns in a tricot pattern and supported by transversely oriented glass fibers for improved handling and manufacturing [3]. The fabric's total areal density is 333 g/m<sup>2</sup>, with carbon fiber tows making up 92.8% of the weight. Flat carbon fiber/epoxy panels (900 mm x 550 mm) were fabricated using HP-RTM with a [0]<sub>7</sub> stacking sequence [4]. The consolidated panel has a volume fraction of 53% and an average thickness of 2.27±0.03 mm. The mechanical properties of the UD-NCF composite material were taken from [5] and are summarized here:  $E_1 = 123.4$  GPa,  $E_2 = 8.4$  GPa,  $\nu_{12} = 0.37$ ,  $G_{12} = 3.4$  GPa,  $X_t = 1765$  MPa,  $Y_t = 60.3$  MPa,  $X_c = 1000.7$  MPa,  $Y_c = 144.9$  MPa, and  $S_{12} = 42.6$  MPa.

Adhesive bonding was achieved using the 3M 07333 Impact Resistant Structural Adhesive (toughened epoxy). The adhesive has a Young's modulus of 2.1 GPa, a Poisson's ratio of 0.43, an elongation at failure of about 2.5%, and an ultimate tensile strength of 35 MPa. The mixed viscosity ranges from 150,000 to 200,000 cPs. The material was cured at 80°C for 90 minutes, followed by a 30-minute cooling period, as recommended by the manufacturer to ensure maximum adhesive strength and reduce variability.

### 2.2 Surface preparation and characterization

Sanding was performed using 400-grit aluminum oxide sandpaper (Norton Saint-Gobain) under two conditions based on sanding time as described in [2]. The first condition involved sanding for 1 minute, with 30 seconds clockwise and 30 seconds counterclockwise (S1). The second condition involved sanding for 2 minutes, with 1 minute each clockwise and counterclockwise (S2). Degreasing with acetone was done before and after sanding to clean the substrates and remove debris. A baseline surface was established by degreasing the as-received material for comparison. Surface roughness of the CFRP before and after preparation was measured using Laser Scanning Confocal Microscopy (KEYENCE VK-X250, Canada). Measurements were taken at various locations on the target surface to highlight CFRP surface features before and after treatment.

Advancing and receding contact angles (i.e., A.C.A and R.C.A.) were determined using a contact angle goniometer (RAME-Hart Instrument Co. Model: 190 C.A.) [2]. By increasing the droplet volume, the contact angle of the drop will increase, and the contact line remains pinned until the A.C.A. is reached. Similarly, by decreasing the drop volume, the contact line will remain pinned and the shape of the drop changes until the R.C.A. is reached.

### 2.3 Mechanical testing methods

DCB and ENF tests were conducted using CFRP substrates obtained by cutting composite plates with an abrasive water jet cutter and treated as described in Section 2.2. These substrates, with dimensions of length  $L=140$ mm and width  $B=25.4$ mm, were individually prepared and joined in a mold using the toughened epoxy adhesive. Bondline thickness was maintained at 0.25 mm using shims, positioned at the starter-crack region and the test sample's end. After removal from the mold, excess adhesive was cleaned from the side surfaces, which were then painted white with vertical lines to aid visualization of crack growth. For DCB testing, loading blocks were bonded onto CFRP surfaces using a fast-curing adhesive (LOCTITE 480 PRISM). Mechanical tests utilized a servo-hydraulic test frame with an MTS Flex Test SE controller. A test frame provided with a 2.2 kN load cell was used for DCB tests, while for ENF tests, the three point bending fixture was mounted on a frame provided with a 5 kN load cell. An overview of both test set-up is shown in Fig. 1 [2]. CCD cameras were used to monitor crack propagation

CANCOM2024 – CANADIAN INTERNATIONAL CONFERENCE ON COMPOSITE MATERIALS

and to supply localized views of the specimen. Loading in DCB tests occurred at a displacement rate of 0.1 mm/s. The same rate was used for the ENF tests. The toughness was determined using the following relations:

$$G_{Ic} = \frac{6P^2}{B^2h} \left( \frac{2a_e^2}{E_f h^2} + \frac{1}{5G_{12}} \right) \quad (1a)$$

$$G_{IIc} = \frac{9P^2 a_e^2}{16E_f B^2 h^3} \quad (1b)$$

Where  $G_{Ic}$  and  $G_{IIc}$  are the Mode I and Mode II toughness of the adhesive;  $P$  is the applied load,  $a_e$  is the equivalent crack length which accounts for the fracture process zone effect at the crack tip, while  $E_f$  is the corrected flexural modulus of the specimen [7]. Post-failure observations of the fractured surfaces were carried out with a Keyence VHX-5000 Opto Digital Microscope (Canada).



Figure 1. Experimental set-up employed employed in the present study and available at University of Waterloo E3-2106. (a) DCB and (b) ENF tests. The servo-hydraulic test frame was provided with an MTS Flex Test SE controller.

## 3 RESULTS

### 3.1 Surface morphology and wettability of the laminates

Microscopy images of the treated surfaces are shown in Fig. 2(a). The original as-produced surface (“as is”) appears relatively smooth, and the presence of polyester stitches can be readily observed from visual inspection since the epoxy matrix was optically translucent. After sanding (S1), the stitches seem to be still embedded within a thin epoxy layer, while the glass fibers become more visible. With prolonged standing (S2), the glass fibers are further exposed, and so are the carbon fibers, although they appear to be well anchored to the epoxy matrix.

To further assess the surfaces before bonding, the wettability was analyzed using A.C.A. and R.C.A. [6]. As shown in Fig. 2(b), the R.C.A. was somewhat difficult to determine with accuracy because the contact line remained pinned until the receding angle was too small to be measured accurately. Instead, the A.C.A. was most reproducible, also with respect to the static measurement. The A.C.A. values for S0, S1 and S2 are reported in Fig. 2(c). The inset figure shows the superposition of two snapshots that highlight the movement of the contact line and the achievement of the A.C.A.. Interestingly, the A.C.A. of all samples is relatively stable and increases slightly after sanding. The average values, which are included in Fig. 2(c) indicate that the initial hydrophobic surface remains so after sanding. A potential reason for such behavior could be associated to the polyester stitches used to hold the layers of the non-crimp fabric. These may create discontinuities in the surface, making it challenging for epoxy adhesives to wet the substrate uniformly. Moreover, glass fibers and polyester stitches may have different chemical

CANCOM2024 – CANADIAN INTERNATIONAL CONFERENCE ON COMPOSITE MATERIALS

compositions and surface energies, posing challenges for achieving strong adhesion with epoxy adhesives, which require compatibility at the molecular level. Further evaluations of the surface preparation methods were made directly performing mechanical tests. To this aim, the sanding treatment S1 was selected since there was no major difference in the surface metrics and topography of S1 and S2.

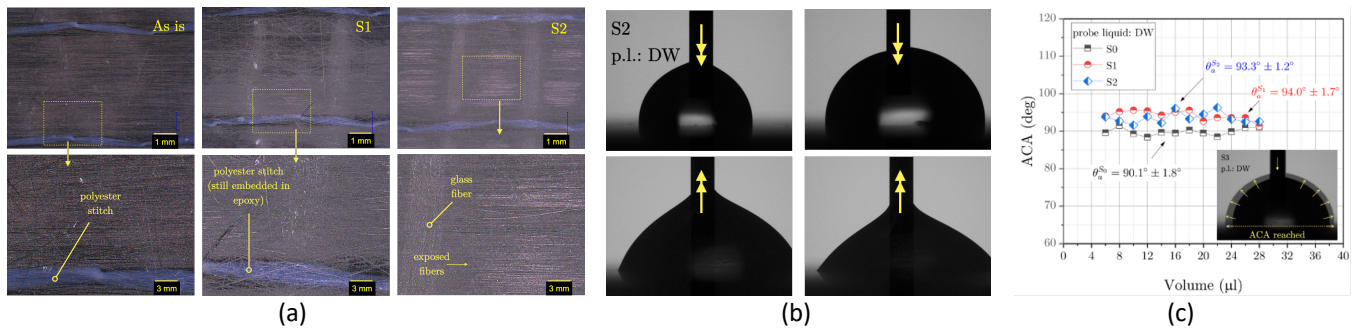


Figure 2. (a) Optical microscopy images of the composite surface before and after sanding. (b) Snapshots taken during measurement of advancing (top) and receding (bottom) contact angles on surface S2. (c) Advancing contact angles as a function of the droplet volume (after corrections using Wenzel’s equation [2]). Probe liquid: distilled water.

### 3.2 Fracture tests

The load-displacement responses and R-curves of DCB specimens treated with sanding are depicted in Fig. 3(a) and (b). Considering the common scattered response of CFRP/epoxy joints [6], the reported results remain consistent. In all trials, the load increases linearly, peaks, and then initiates macroscopic crack propagation (softening), leading to gradual load reduction with increasing displacement. DCB tests ceased when the crack reached about 80% of the bonded region, and the remaining bondline was fractured with a wedge. Fluctuations in load during softening mainly correspond to the crack path. Crack growth can involve cohesive fracture of the adhesive, mixed failure of the CFRP substrates (involving intralaminar and interlaminar fracture) or both [8].

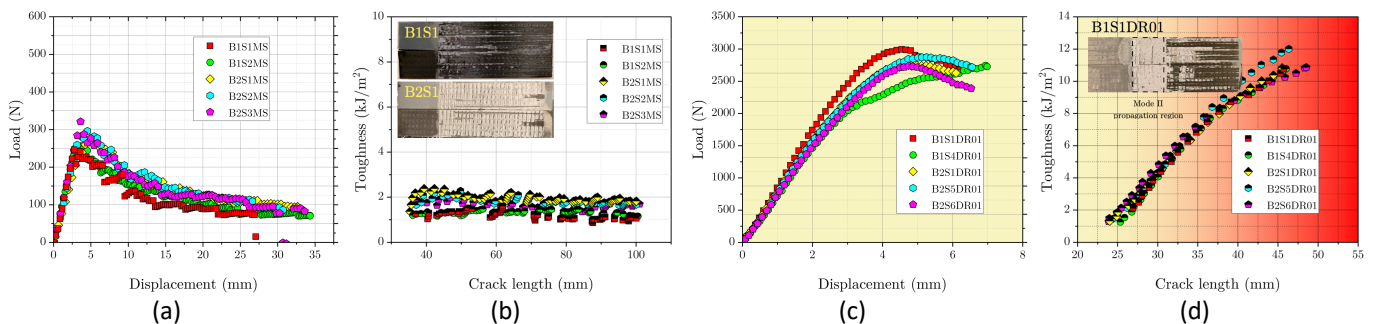


Figure 3: (a) Load-displacement responses recorded in DCB tests; MS stands for manual sanding. (b) R-curves determined in DCB tests. (c) Load-displacement curves recorded in Mode II fracture tests; DR01 stands for displacement rate at 0.1 mm/s. (d) R-curves determined in ENF tests. The insets show instances of DCB and ENF fractured surfaces.

The associated R-curves of DCB specimens appear relatively flat, indicating consistent fracture toughness across the bonded area. Visual inspection revealed that cohesive fracture of the epoxy adhesive was the primary failure mechanism in all tests except B1S1, which displayed a mixture of cohesive fracture of the epoxy and fracture of the

CANCOM2024 – CANADIAN INTERNATIONAL CONFERENCE ON COMPOSITE MATERIALS

outmost region of the composite substrate (mainly interlaminar). Examples of both mechanisms are shown in the insets of Fig. 3(b) and the corresponding toughness was  $(1.14 \pm 0.16)$  kJ/m<sup>2</sup> (interlaminar) and  $(1.95 \pm 0.17)$  kJ/m<sup>2</sup> (cohesive fracture of the adhesive), which are in excellent agreement with those reported by Dehaghani [5]. The average toughness obtained herein is  $\cong 1.5$  kJ/m<sup>2</sup>. This value is deemed satisfactory and is larger than that reported in previous work for bonded CFRPs comprising the Araldite 420 A/B (Huntsman) toughened epoxy [6].

ENF test results are depicted in Fig. 3(c) and exhibit consistent initial linear responses across all tests, with deviations observed post-macroscopic crack formation. The most significant deviation occurred during testing of B1S4DR01, which was attributed to fracture of the CFRP after visual inspection of fractured surfaces. Tests were halted as crack fronts approached the loading pin location, preventing further loading to avoid bulk damage to the upper CFRP substrate. Corresponding R-curves in Fig. 3(d) remained consistent and comparable. However, none of the tests achieved steady-state crack growth, as the R-curve consistently rose with crack length. Hence, only initiation fracture toughness was provided for each ENF test. The average toughness, excluding B1S4DR01, was  $(1.28 \pm 0.05)$  kJ/m<sup>2</sup>. Following mechanical testing, the samples were separated using a wedge, and an inspection of the fracture surfaces revealed a dominant cohesive fracture in the crack propagation region, as shown in the inset of Fig. 3(d).

### 3.3 Analysis of fractured surfaces

A more detailed examination of the failure process involved capturing CCD images in situ during mechanical tests and utilizing images obtained via an optical microscope. These results are presented in Fig. 4. As previously mentioned, cohesive fracture of the adhesive layer predominated in most DCB specimens, except for B1S1MS, which experienced failure of the CFRP substrates (mainly interlaminar), as depicted in Fig. 4(a). For the remainder of the DCB specimens, a representative image of the fractured surfaces is provided in Fig. 4(b). Close observations reveal the exposure of glass fibers, polyester stitches, and carbon fibers. Furthermore, the images confirmed weak adhesion at epoxy/glass and epoxy/polyester interfaces, evident from their exposed state with minimal epoxy traces (though epoxy presence cannot be completely ruled out based solely on visual inspection). Additionally, the imprint of glass fibers from the mating substrate is visible. Small spots of substrate fracture observed in all specimens confirm that such fractures involve peeling of small portions of the outermost surface layers of CFRP.

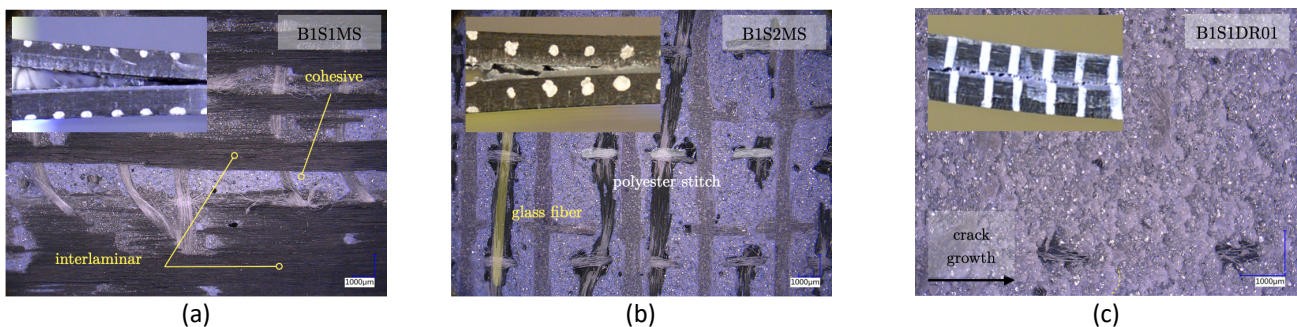


Figure 4: Typical images of crack propagation taken in situ using a CCD camera, and corresponding fracture surfaces. The images refer to (a) interlaminar fracture in a DCB specimen; (b) cohesive fracture in a DCB; (c) cohesive fracture associated to Mode II crack propagation in a ENF test.

Fracture surface inspection of ENF samples revealed disparities compared to Mode I tests. Regions exhibiting cohesive fracture did not show the noticeable lack of adhesion at glass fiber/epoxy interfaces observed in DCB tests. Glass fibers and/or their imprint were not easily discernible on these fracture surfaces. Moreover, shear fracture

## CANCOM2024 – CANADIAN INTERNATIONAL CONFERENCE ON COMPOSITE MATERIALS

mechanisms differed, dominated by ductile fracture with parabolic microcracks, attributed to intense plastic (shear) straining of the adhesive layer, as seen in Fig. 4(c). Notably, the rubber-modified 3M 07333 epoxy consists of an epoxy matrix with dispersed synthetic rubber. During straining, rubber can form micro-voids that grow through plastic deformation and coalesce until final fracture. Interestingly, a substantial process zone was observed in ENF tests, as shown in the inset of Fig. 4(c).

## 4 CONCLUSIONS

The results of mechanical tests revealed that differences in chemical composition and surface energies between glass fibers, polyester stitches, and epoxy may hinder strong adhesion, as epoxy adhesives typically require molecular-level compatibility. Additionally, the mechanism of failure and the interaction between the advancing crack and the composite structure depend on the loading mode. Mode II tests did not exhibit significant exposure of glass fibers or polyester stitches, as observed in Mode I tests. A large fracture process zone ahead of the crack tip was also observed, characterized by localized cavitation, microcrack growth, and ductile shear deformation. Overall, the interaction between the adherend's microstructure and composition significantly influenced the adhesion process and fracture behavior observed. The effect was also compounded by the mode of loading. Understanding these interactions is crucial for optimizing adhesive bonding techniques and enhancing the reliability of composite structures in diverse applications.

## 5 REFERENCES

- [1] S. Das, D. Graziano, V. K. K. Upadhyayula, E. Masanet, M. Riddle, and J. Cresko, "Vehicle lightweighting energy use impacts in U.S. light-duty vehicle fleet," *Sustain. Mater. Technol.*, vol. 8, pp. 5–13, 2016, doi: 10.1016/j.susmat.2016.04.001.
- [2] T. Gao. Adhesive bonding of polymer composites reinforced with carbon unidirectional non-crimp fabrics. MAsc Thesis, University of Waterloo, 2022.
- [3] M. Ghazimoradi, E.A. Trejo, C. Butcher, J. Montesano. Characterizing the macroscopic response and the local deformation mechanisms of a unidirectional non-crimp fabric. *Compos. Part A Appl. Sci. Manuf.*, vol. 156, pp 106857, 2022.
- [4] A. Cherniaev, Y. Zeng, D. Cronin, J. Montesano. Quasi-static and dynamic characterization of unidirectional non-crimp carbon fiber fabric composites processed by HP-RTM. *Polymer Testing*, vol. 76, pp 365-375, 2019.
- [5] R. Chitsaz Dehaghani. Experimental and Numerical Assessment of Adhesively Bonded Non-Crimp Fabric Carbon Fiber/Epoxy Composite Joints. MAsc Thesis, University of Waterloo, 2020.
- [6] R. Tao, M. Alfano, and G. Lubineau, "Laser-based surface patterning of composite plates for improved secondary adhesive bonding," *Compos. Part A Appl. Sci. Manuf.*, vol. 109, no. February, pp. 84–94, 2018, doi: 10.1016/j.compositesa.2018.02.041.
- [7] M.F.S.F. de Moura, J.J.L. Morais, N. Dourado, A new data reduction scheme for mode I wood fracture characterization using the double cantilever beam test, *Eng Frac Mech*, vol. 75, Issue 13, 2008.
- [8] C. Morano, R. Tao, M. Alfano, and G. Lubineau, "Effect of mechanical pretreatments on damage mechanisms and fracture toughness in cfrp/epoxy joints," *Materials*, vol. 14, no. 6, pp. 1–16, 2021, doi: 10.3390/ma14061512.